Exploration Geophysics

SUBSURFACE ATTENUATION ESTIMATION USING A NOVEL HYBRID METHOD BASED ON FWE FUNCTION AND POWER SPECTRUM

Journal:	*Exploration Geophysics*
Manuscript ID	EG16022.R3
Manuscript Type:	Research Paper
Date Submitted by the Author:	24-Jan-2017
Complete List of Authors:	Li, Jingnan; Sinopec Geophysical Research Institute; China University of Petroleum Beijing, College of Geophysics and Information Engineering Wang, Shangxu; China University of Petroleum (Beijing), Department of Geophysics and Information Yang, Dengfeng; The Research Institute of CNOOC (China) Ltd. Shenzhen Tang, Genyang; China University of Petroleum Beijing, College of Geophysics and Information Engineering Chen, Yangkang; The University of Texas at Austin, Bureau of Economic Geology
Keyword:	Attenuation, Q, Estimation

SUBSURFACE ATTENUATION ESTIMATION USING A NOVEL HYBRID METHOD BASED ON FWE FUNCTION AND POWER SPECTRUM

Li Jingnan
Sinopec Geophysical Research Institute, 219 Shanggao Road, Jiangning, Nanjing, Jiangsu China 211103 (presently)
China University of Petroleum-Beijing, 18 Fuxue Road, Changping, Beijing China 102249 (previously)
E-mail: li.jnan@163.com

Wang Shangxu
China University of Petroleum-Beijing, 18 Fuxue Road, Changping, Beijing China 102249
Phone: +86-89733364
Facsimile: +86-89733364
E-mail: wangsx@cup.edu.cn

Yang Dengfeng
The Research Institute of CNOOC (China) Ltd. Shenzhen, Guangzhou China 510240
E-mail: yangdfdqwl@163.com

Tang Genyang* (corresponding author)
China University of Petroleum-Beijing, 18 Fuxue Road, Changping, Beijing China 102249
E-mail: tanggenyang@163.com

Chen Yangkang
The Jackson School of Geosciences, The University of Texas at Austin, Austin, TX 78713-8924 USA

E-mail: ykchen@utexas.edu

Date: Manuscript received on January 23, 2017 revised on 23 January, 2017

Left Running Heading: Li, Wang, Yang, Tang and Chen

Right Running Heading: *Q* estimation using FWE function and power spectrum

ABSTRACT

Seismic waves propagating in subsurface suffer from attenuation, which can be represented by quality factor Q. Knowledge of Q plays a vital role in hydrocarbon exploration. Many methods to measure Q have been proposed, among which the central frequency shift (CFS) and the peak frequency shift (PFS) are two commonly used ones. However, both methods are under the assumption of a particular shape for amplitude spectra, which will cause systematic error in Q estimation. Recently a new method to estimate Q has been proposed to overcome this disadvantage by using frequency-weighted-exponential (FWE) function to fit amplitude spectra of different shapes. In the FWE method, a key procedure is to calculate the central frequency and variance of amplitude spectrum. However, the amplitude spectrum is susceptible to noise, whereas the power spectrum is less sensitive to random noise and has better anti-noise performance. To enhance the robustness of the FWE method, we propose a novel hybrid method by combining the advantage of the FWE method and the power spectrum, which is called the improved FWE method (IFWE). The basic idea is to consider the attenuation of power spectrum instead of amplitude spectrum and to use a modified FWE function to fit power spectra, according to which we derive a new Q estimation formula. Tests of noisy synthetic data show that the IFWE are more robust than the FWE. Moreover, the frequency bandwidth selection in the IFWE can be more flexible than that in the FWE. The application to field VSP data and surface seismic data further demonstrate its validity.

Key Words: Attenuation, Q factor, FWE function, power spectrum.

INTRODUCTION

Due to anelasticity and inhomogeneity of earth media, seismic waves propagating in subsurface undergo attenuation, which causes energy dissipation and velocity dispersion. Energy dissipation means that amplitudes of seismic waves decay over time and traveling distance, with high-frequency components attenuating more rapidly than those of low-frequency components, which in turn narrows the frequency bandwidth. On the other hand, velocity dispersion denotes that different frequency components have different propagation velocities, thus delaying and stretching seismic waves (Chai et al., 2014). In combination, these effects decrease the resolution of seismic data, make the imaging and interpretation of the subsurface more difficult, and obscure quantitative analysis of amplitude variation with offset (AVO) (Mittet et al., 1995; Yan and Liu, 2009; Reine et al, 2012).

Seismic attenuation can be quantified by a dimensionless quality factor, Q. Determination of Q for earth media is of great importance in the processing and interpretation of seismic data. If Q of each stratigraphic layer is available, one can apply absorption compensation (Wang, 2002, 2006; Wang and Chen, 2014) to seismic data so as to enhance resolution of seismic imaging, which can make structural interpretation and AVO analysis more accurate (Li et al., 2015). Both field and laboratory measurements show that Q is related to lithology, porosity, permeability, fluid types and fluid saturation (Johnston et al., 1979; Winkler and Nur, 1982; Best, 1997). Different rock and fluid contents may be represented by Q variation (Dasgupta and Clark, 1998); thus Q can be an indicator of reservoir fluid. Therefore, Q measurement can be a useful tool for seismic interpretation and reservoir characterization.

Many approaches to extract Q factor have been proposed. Currently, the common methods are formulated in the frequency domain, such as the logarithmic spectral ratio method (LSR) (Tonn, 1991), the central frequency shift method (CFS) (Quan and Harris, 1997) and the peak frequency shift method (PFS) (Zhang and Ulrych, 2002), all of which have advantages as well as limitations. The LSR performs well in the case of noise-free data but it is easily affected by noise (Tonn, 1991). In comparison to the LSR, the CFS and the PFS have errors even for noise-free data due to the assumption on the particular shape of amplitude spectra. However, the estimation with the CFS is more reliable when the noise level is high (Picotti and Carcione, 2006) and it has higher robustness in such condition. This is due to the fact that the CFS makes use of the statistic attribute of amplitude spectrum. On the other hand, the CFS does not require a complete spectrum for Q calculation that is necessary for the LSR (Quan and Harris, 1997), and it only need a reference frequency. By saying "complete spectrum", we mean that the LSR requires the knowledge of spectra for frequencies within the bandwidth of seismic data as reference for the calculation of spectra ratio. Therefore, these current methods often make a trade-off between accuracy and robustness.

Li and Liu (2015) recently used a frequency-weighted-exponential (FWE) function (Hu et al., 2011) to fit various amplitude spectra, and then developed a novel and promising Q estimation approach, which is called FWE method. The FWE method has an advantage that it is independent of the type of source wavelet. In this approach, the calculation of the central frequency and variance of amplitude spectrum are of great importance. Thus, the FWE method has some same limitations as the CFS does. One of the limitations is on the choice of frequency band for noisy data (Wang et al., 2015; Li et al., 2016b). The common practice is to take many trials before finding a desired bandwidth, or to use an empirical effective-bandwidth coefficient λ to determine the bandwidth (Hu et al., 2013). However

the choice of λ is empirical and can be different for various situations. Wang (2015) has proved that the central frequency is close to the mean frequency evaluated from the power spectrum rather than the amplitude spectrum for Ricker wavelet. In addition, we find that the power spectrum of a signal is less susceptible to random noise than its amplitude spectrum for different types of wavelets. Thus it is better to use the power spectrum in the Q estimation. By combining the advantages of the FWE function and the power spectrum, we propose an improved FWE method (IFWE) to extract Q factors. The validity, effectiveness and anti-noise capability of the proposed method are tested using both noise-free and noisy synthetic data. The application to field data further confirms the feasibility and robustness of the proposed method.

THEORY AND METHODS

The quality factor Q is often assumed to be independent of the frequency within seismic frequencies (Attewell and Ramana, 1966; Kjartansson, 1979). The causal constant Q model of Futterman (Futterman, 1962) is widely used. Based on this model, if we only consider the attenuation of the amplitude spectrum of seismic wave, the attenuation mechanism can be written as

$$A_2(f) = C \cdot A_1(f) \exp\left[-\frac{\pi f \Delta t}{Q}\right] \tag{1}$$

where $A_2(f)$ is the amplitude spectrum of the received signal; $A_1(f)$ is the amplitude spectrum of the reference signal; strictly speaking C indicates frequency-dependent

attenuation including geometrical spreading and source/receiver transfer function, however we make a simplification in the later derivations by assuming C frequency-independent as many proposed methods such as the LSR, CFS and PFS. Δt is the time difference between the received signal and the reference signal.

Original FWE Function Fitting Method

In the proposed method, Li and Liu (2015) fitted various wavelets by the FWE function (Hu et al., 2011), which is expressed as

$$W(f) = Af^n \exp\left(-\frac{f}{f_b}\right) \tag{2}$$

where A is an amplitude scaling constant; n is the symmetry index that controls symmetry property; f_b is the bandwidth factor that controls bandwidth.

After fitting reference signal and attenuation signal with FWE function, they build a relation between the attenuation amplitude spectrum and the original amplitude spectrum in the form of Eq. 1. Finally they derive a new Q extraction formula

$$Q = \frac{\pi \Delta t f_{b1} f_{b2}}{f_{b1} - f_{b2}} \quad . \tag{3}$$

where f_{b1} and f_{b2} are the bandwidth factors of the reference signal and the received signal, which are calculated as

$$f_{bi} = \frac{\sigma_i^2}{f_{ci}^2}, \quad i = 1, 2 \tag{4}$$

f_{ci} and σ_i^2 (i = 1, 2) are the central frequency and variance of the reference and attenuated amplitude spectra, which are defined as

$$f_{ci} = \frac{\int_0^\infty fW(f)df}{\int_0^\infty W(f)df} \tag{5}$$

$$\sigma_i^2 = \frac{\int_0^\infty (f - f_c)^2 W(f)df}{\int_0^\infty W(f)df} \tag{6}$$

Improved FWE Method Based On Power Spectrum

The calculation of central frequency (f_c) is a critical step in the above spectra fitting method, which is performed in the amplitude spectra. However, Wang (2015) has proved that for Ricker wavelet, the central frequency (f_c) is close to the mean frequency evaluated from the power spectrum rather than the amplitude spectrum. It is widely recognized that the autocorrelation function (ACF) improves periodic events but not random noise (the Fourier transform of ACF is the power spectrum). We also give an explicit illustration in Appendix A. Based on this property, we derive a power spectra fitting method to extract the Q factor, which is called improved FWE method. Note that the applicability of the proposed method is limited to the random noise case.

We assume that an arbitrary amplitude spectrum can be fitted by the FWE function, then its power spectrum can be fitted by

$$E(f)=\left[W(f)\right]^2=A^2 f^{2n}\exp\left(-\frac{2f}{f_b}\right) \tag{7}$$

We can compute the central frequency of the power spectrum as

$$f_c=\frac{\int_0^\infty fE(f)df}{\int_0^\infty E(f)df}=\frac{(2n+1)}{2}f_b \tag{8}$$

and its variance as

$$\sigma^2=\frac{\int_0^\infty (f-f_c)^2 E(f)df}{\int_0^\infty E(f)df}=\frac{2n+1}{4}f_b^2 \tag{9}$$

Then, we fit the power spectrum of an arbitrary wavelet by using $E(f)$. According to Eqs. 8 and 9, n and f_b can be obtained by calculating the central frequency and variance of the power spectra,

$$\begin{cases} n=\frac{1}{2}\left(\frac{f_c^2}{\sigma^2}-1\right) \\ f_b=\frac{2\sigma^2}{f_c} \end{cases} \tag{10}$$

If the power spectrum of the original wavelet satisfies $E(f)$, according to Eq. 1 the attenuated power spectrum is

$$E^a(f,t) = \left[CW(f)\exp\left(-\frac{\pi f \Delta t}{Q}\right)\right]^2$$
$$= C^2 A^2 f^{2n} \exp\left(-\frac{2f}{f_b}\right)\exp\left(-\frac{2\pi f \Delta t}{Q}\right) \quad (11)$$
$$= C^2 A^2 f^{2n} \exp\left[-2f\left(\frac{1}{f_b}+\frac{\pi\Delta t}{Q}\right)\right]$$

Thus the bandwidth factor of attenuated power spectrum is

$$f_b^a = \frac{1}{\frac{1}{f_b}+\frac{\pi\Delta t}{Q}} \quad (12)$$

Therefore, we can obtain the relationship between Q and bandwidth factor according to Eq. 12

$$Q = \frac{\pi\Delta t f_b f_b^a}{f_b - f_b^a} \quad (13)$$

We see that this formula happens to be the same with Eq. 3 in form. However by contrasting Eqs. 4 and 10, we observe that the calculations of bandwidth factors are different for the two methods.

The above equation requires that the symmetry index remains invariant. This condition is hardly satisfied for a source wavelet whose shape of the amplitude spectrum is a nonstandard FWE function. To solve this problem, we take an average of the symmetry indices of the source and attenuated wavelets. Note that this processing can cause some error, as also stated in the FWE method (Li and Liu, 2015). Accordingly, we recalculate the bandwidth factors as follows,

,

$$\begin{cases} \overline{n} = \dfrac{n + n^a}{2} \\ f_b^{'} = \dfrac{2 f_c}{2\overline{n} + 1} \\ f_b^{a'} = \dfrac{2 f_c^a}{2\overline{n} + 1} \end{cases} \tag{14}$$

Finally, Q can be estimated as

$$Q = \frac{\pi t f_b^{'} f_b^{a'}}{\left(f_b^{'} - f_b^{a'} \right)} \tag{15}$$

Then we can compute Q based on (15) and (14).

NUMERICAL EXAMPLES

In the following we use similar tests to those in Li et al (2016b) to examine the validity and anti-noise capability of the IFWE method.

Validity Of IFWE

We examine the feasibility of the IFWE in homogeneous viscoelastic medium using synthetic examples. We choose four Q values for the tests, namely Q = 25, 50, 100, and 150, which represent strong (25), moderate (50 and 100) and weak attenuation (150). As the Ricker wavelet is closer to real situation when seismic waves propagate in subsurface medium and is often used in seismic analysis (Wang 2015; Li et al., 2015), a Ricker wavelet with a dominant frequency of 40 Hz is employed in the synthetic tests. The time difference between the first

and second waveform for every trace in Fig. 1 is 0.3 s. Then we generate synthetic data in frequency domain. The frequency spectra of the Ricker wavelet is calculated through Fourier transform. Then we use Eq. 1 to synthesize attenuation spectra at the frequencies within the bandwidth of the Ricker wavelet. The synthetic data considering attenuation in time domain are then obtained by computing the inverse Fourier transform of attenuation spectra, as displayed in Fig. 1a. Then we use the IFWE to estimate Q from the synthetic data considering attenuation, with the FWE and CFS as comparisons. The frequency bandwidth used in the Q estimation is 0-100 Hz. The estimation results are shown in Table 1. We see that the results using the FWE and IFWE are more accurate than those using the CFS. The relatively large deviation from true Q values using the CFS is derived from the assumption of a Gaussian shaped amplitude spectrum for both the reference and received waveform, which is not true for Ricker wavelet. However, such assumption is unnecessary in the FWE method and the IFWE method. The FWE function or its square is used to fit various amplitude spectra or power spectra, which helps to overcome the disadvantage of the CFS in some sense and thus have better performance. However the FWE and the IFWE are limited to fitting accuracy of amplitude spectra and power spectra respectively. The processing in Equation (14) can bring some error for the IFWE, as also stated in the FWE method (Li and Liu, 2015). Synthetic tests of Ricker wavelet show that the IFWE is slightly more accurate than the FWE. To test the influence of wavelet types on the Q estimation, we further test two other wavelets, formulated by the first and third derivative of a Gauss function, which are called Gauss 1 and Gauss 3 wavelet here. The parameters except the wavelet type are the same with the above test. The corresponding attenuation seismograms are shown in Figs. 1b and 1c, respectively. The estimated results are shown in Table 1. We see that for Gauss 1 wavelet, the IFWE is a bit worse than the FWE. Whereas for Gauss 3 wavelet, the IFWE is slightly better than the FWE. This may be due to that for different

wavelets, the fitting of amplitude spectrum and power spectrum has slight different accuracy. Considering that the difference of the estimation results is small, we may conclude that the accuracy of the IFWE and FWE is on a similar level.

We also test the performance of the methods shown above with increasing travel time. In the tests, the true Q is 100. The travel time increases from 0.2 s to 1.2 s with 0.2 s interval. We respectively use the above three wavelets to synthesize attenuation data, as shown in Fig. 2. Then we employ a 100 ms time window to extract the waveforms at different travel time. Using the extracted attenuated waveforms and the original wavelet, we can calculate the corresponding Q values with the CFS, the FWE and the IFWE. The frequency bandwidth in the Q estimation is also 0-100 Hz. The estimated Q are listed in Table 2. We can see that the estimation errors increase with increasing travel time for all the three approaches. The waveform has larger deviation from Gauss spectrum with increasing travel time, causing the reduction of estimation accuracy for the CFS. However, the FWE and IFWE have much higher accuracy than the CFS. This is because the two methods are to some extent independent of the spectrum shape of waveform. The processing in Eq. 14 can cause larger error in the Q estimation with increasing travel time of seismic wave for the IFWE method. A similar analysis is made in Li and Liu (2015) for the FWE method. Moreover, the IFWE is more accurate than the FWE when using the Ricker wavelet and Gauss 3 wavelet, but slightly less accurate than the FWE when using the Gauss 1 wavelet. This may be due to that the fitting accuracy of amplitude spectrum and power spectrum is slightly different for different wavelets, as illustrated above.

Anti-noise Capability Of IFWE

Real data is always contaminated by noises, which will bring difficulty to Q estimation and influence the robustness of estimation. Thus the stability in evaluating the Q factor is of great importance when the data is polluted by noise (Li et al., 2015).

Gaussian random noises

First, we use noisy data with different signal-noise-ratios (SNRs) to test the robustness of the methods. The wavelets and travel time are the same as those in the first test (Table 1). Different noise levels of white Gaussian random noises are added to the noise-free synthetic data. The true Q value is 100. The selected frequency band in the Q estimation is 5-100 Hz. For each SNR, 1000 independent realizations are performed. We then compute the mean values and standard deviations of the estimated Q to show their statistical performances.

Firstly, we use synthetic data with a relatively high SNR and a relatively low SNR, namely 20 dB and 10 dB, to calculate Q values. The noisy attenuation data for Ricker wavelet, Gauss 1 wavelet and Gauss 3 wavelet are shown in Figs. 3a, 3b and 3c respectively. The probability distributions of the estimated Q using both the IFWE and the FWE are shown in Figs. 4, 5 and 6 respectively. For all the three wavelets, the corresponding Q estimations have similar performance. When SNR = 20 dB, the estimated Q of both methods has narrow deviation and small errors. When SNR = 10 dB, the performance of both methods deteriorates as the estimation has wider deviation and larger errors. However, for each noise level, the

histogram for IFWE shows a more peaked distribution compared with that for FWE; the mean values u with the IFWE are closer to true Q value and the standard deviations σ are smaller than those with the FWE. This indicates that Q estimation using the IFWE has better stability than that using the FWE for all the three wavelets we test.

Secondly, noisy data with various SNRs that vary from 5 to 40 dB are used to estimate the Q value. To avoid redundancy, we only show the estimated result for the Ricker wavelet. For each SNR, 1000 independent realizations are performed. Fig. 7 shows the mean values and standard deviations of the estimated Q for different SNRs. We see that the estimation results of both FWE and IFWE become less accurate with increasing noise levels. The performance of the FWE significantly deteriorates whereas the performance of the IFWE is much better than the FWE. The mean values of the IFWE are closer to true value and the standard deviations are much smaller than those of the FWE. This further demonstrates that the IFWE is more robust than the FWE. From Fig. A1, we see that power spectra is less sensitive to random noises than the amplitude spectra. The calculation of the square of amplitude can suppress the effect of noise in the fitting. Therefore the IFWE can produce more reliable results than the FWE for noisy data.

Sinusoidal wave noises

Since it is important to handle anomaly in the frequency domain, we also test the performance of our method when there are interference of sinusoidal waves in the signal. We use the

attenuation data generated by the Ricker wavelet (the third trace in Fig. 1a). Three sinusoidal waves with frequencies respectively 30Hz, 50Hz and 80Hz are added to the noise-free data. The magnitudes of the sinusoidal waves are two times as big as those of the attenuation signal at these three frequencies. Then we use the FWE and IFWE to compute the Q factors. The selected frequency band for Q estimation is 5-100 Hz. The estimated Q are 99.76 and 99.94, respectively. We see that both methods produce good results and the IFWE yield slightly more accurate result. When more frequencies are contaminated by sinusoidal noises, the accuracy of amplitude spectrum and power spectrum fitting using Eqs. (2) and (7) will decrease, causing the reduction of performance of Q estimation for both the FWE and the IFWE. This indicates that the IFWE can have good tolerance to spectrum anomaly at sparse frequencies.

Frequency Band Selection For IFWE

The computation of the central frequency (f_c) and variance (σ^2) of amplitude spectra are crucial in the FWE method. However for noisy data, the computation of the central frequency and variance depends on the choice of frequency band (Wang et al., 2015; Li et al., 2016b). The bandwidth should be neither too narrow nor too wide. With narrowing bandwidth, the performance of statistic attributes of spectra worsens and the robustness decreases. With increasing bandwidth, the signal-to-noise ratio of the data decreases, and thus the accuracy reduces. Therefore for noisy seismic data, it is a critical task to select the optimal frequency band in the FWE method. The magnitudes of high and low frequency components of the signal spectra are usually small and susceptible to noises. If these

contaminated components are included in the frequency band, substantial error will be brought to the Q estimation with the FWE. However, power spectrum is less sensitive to noise interference (see Appendix A). Therefore we can conjecture that the bandwidth selection in IFWE can be more flexible.

To examine the effect of bandwidth choices on Q estimation using both the FWE and IFWE for noisy attenuation data, we calculate Q with different bandwidths. In this test, we choose the data with SNR = 10 dB, 15 dB and 20 dB. The lower limit of frequency band changes from 5 to 30 Hz, and the upper limit from 60 to 130 Hz. First we use the Ricker wavelet to generate the noisy attenuation data, as shown in Fig. 8a. Then we conduct 200 independent realisations for every bandwidth and compute the statistical average as the final estimated Q. For different bandwidths, the relative errors of estimated Q for various SNRs are displayed in Fig. 8. When SNR is relatively high (15 dB and 20 dB), we observe that the estimation errors for FWE are very large in some bandwidths (Figs. 8b and 8d). By contrast, the errors for IFWE are small for most frequency bandwidths (Figs. 8c and 8e). This indicates that the FWE is sensitive to selected frequency bandwidths and different frequency bands will lead to different results, whereas the IFWE is less sensitive to bandwidth selection and different frequency bands have little effect on the estimation results. When the SNR is low (10 dB), the performance of both FWE and IFWE is bad (Figs. 8f and 8g). In this case, IFWE has less strict requirements for bandwidth selections. From this result, we can conclude that the frequency bandwidth selection in IFWE is more tolerant than that in FWE.

Field Data Application

Finally, we test the proposed method using a field zero-offset VSP data set. Fig. 9a displays the original data. The sampling interval is 1 ms. Receivers are placed at depths from 2300 to 4260 m with 10 m depth interval. The type of source is vibroseis, and there is a single source at each cable position. The horizontal offset between the source and the borehole is 50 m. Fig. 9b shows the VSP down-going wavefields after spherical divergence compensation, noise removing, and wavefield separation. We extract the first arrival waveforms (see Fig. 9c) using an 80 ms rectangular window. For two neighbouring first-arrivals, we define the one at shallow location as the reference signal and the one at deep location as the received signal. Then we use the first arrivals to estimate Q with the FWE and IFWE. Figs. 9e and 9f show the estimation results when frequency bandwidths are 3-110 Hz and 3-130 Hz, respectively. Fig. 9g shows the difference of the estimated Q using the above two bandwidths. We observe that the IFWE nearly produces the same results for two different bandwidths whereas the results using the FWE have a difference. This suggests that it is more flexible to choose bandwidth for IFWE than FWE. Although Q values obtained using FWE and IFWE are different, they have a similar trend. The effectiveness of Q estimation can be evaluated using empirical equation $1/Q=(C/v_p)^2$, which describes the relation between the primary velocity v_p and Q factors (Waters, 1978; Udias, 1999). The correlation between Q and velocity have been used to examine whether the estimated Q is reasonable (Blias, 2012; Wang et al., 2015). We then compute the interval velocities from the first arrivals as a comparison with the extracted Q, as displayed in Fig. 9h. We can see that there exists good correlation between the estimated Q factors and interval velocities, indicating validity of the IFWE method. To further verify the effectiveness of the method, we use the estimated Q values to compensate attenuation through the inverse Q filtering. However, we find that the compensation is not obvious (see Fig. 9d, we even

cannot identify the difference of the seismic profiles before and after compensation). The possible reasons may be explained as follows. It is known that the main attenuation comes from near-surface absorption attenuation, however our data is located at relatively deep layers (2300-4260 m). The travel time of seismic wave is also short. In addition, the estimated Q values are relatively large, meaning weak attenuation. These three conditions combine to lead to relatively weak attenuation and thus the compensation performance is not obvious. An obvious compensation can be found in Figures 10 and 13 in Wang (2014), where the field data contains near surface data (50m-1750m) and the attenuation is strong. No oil or gas is found in the detecting area. The estimated results by the two methods are relatively large Q values, which are consistent with the reality. This can further demonstrate the feasibility of the IFWE method.

We also use a surface seismic data set to test the proposed method. Figure 10a shows a post-stack seismic section after some conventional processing (geometrical divergence correction, denoising, etc). We choose the 12th trace from the section (see Figure 11a) and compute its time frequency amplitude spectrum using wavelet transform, as shown in Figure 11b, from which an obvious decrease in dominant frequency can be seen. To facilitate the Q estimation, we refer to Raji and Rietbrock (2013) to divide the data into four parts (see Figure 11a) and assume that each part has a same Q value. The frequency spectra at 100 ms, 330 ms, 530 ms, 620 ms and 840 ms are selected in Q estimation. The frequency bandwidth used in Q estimation is 5-90 Hz. Then we calculate the power spectra within the selected bandwidth at these five time, which are used to estimate Q values in the IFWE method. The estimation results are shown in Figure 11c. Using the estimated Q values, we apply inverse Q filtering to the field seismic data. The compensation results are shown in Figure 10b. Generally, a clear

improvement in the seismic resolution can be observed. We observe that the lateral continuity for events near 0.2 s are improved. The events at 0.6 s to 0.9 s become clearer, which can aid with a better description of structures. The results can further demonstrate the viability of the IFWE method.

Here we test the application of the IFWE to a VSP data set and a surface seismic data set that have relatively high SNR. For more challenging field data such as surface seismic data with small SNR (less than 10 dB or even smaller), the proposed method may also cause large error like the other methods (LSR and CFS). It can be a great challenge to process the seismic reflection data. Many factors (such as noises, multiples, processing procedures and so on) will influence the final Q estimation results. Moreover, the scattering effect is very difficult to overcome. In this case, it is better to use attenuation attribute to evaluate apparent attenuation effects of reflection data, which is useful and promising for hydrocarbon detection and reservoir characterization (Li et al 2016a).

CONCLUSIONS

In this paper, we propose an improved Q estimation method – IFWE. By combining the advantages of the FWE method and the power spectrum, the IFWE can give more stable and more reliable Q estimation for noisy data (note that the applicability of the proposed method is limited to the random noise case). For noise-free attenuation data synthesized by different wavelets, the estimations of the IFWE are close to those of the FWE. But for noisy

synthetic data, the IFWE shows better robustness than the FWE. And it is less sensitive to the bandwidth selection than the FWE. The application to real VSP data and surface seismic data further demonstrate the validity of the IFWE. Since the IFWE has better anti-noise capability and less dependence on bandwidth selection, it can be a helpful tool in estimating Q values in real data.

ACKNOWLEDGEMENTS

This research is supported by the National Key Basic Research Development Program (2013CB228600), National Natural Science Foundation of China (41304042) and Science Foundation of China University of Petroleum, Beijing (2462013BJRC004). We would like to thank Huijuan Song for providing the field seismic data. We are very grateful to the associate editor Shohei Minato and three anonymous reviewers for constructive comments and suggestions, which help greatly to improve the quality of this paper.

REFERENCES

Attewell, P.B., and Ramana, Y.V., 1966, Wave attenuation and internal friction as functions of frequency in rocks: *Geophysics*, **31**, 1049–1056.

Blias, E., 2012, Accurate interval Q-factor estimation from VSP data: *Geophysics*, 77, WA149-WA156.

Best, A., 1997, The effect of pressure on ultrasonic velocity and attenuation in near-surface sedimentary rocks: *Geophys. Prospect.*, **45**, 345-364.

Chai, X., Wang, S., Yuan, S., Zhao, J., Sun, L. and Wei, X., 2014, Sparse reflectivity inversion for nonstationary seismic data: *Geophysics*, **79**, V93-V105.

Dasgupta, R. and Clark, R. A., 1998, Estimation of Q from surface seismic reflection data: *Geophysics*, 63, 2120-2128.

Futterman, W. I., 1962, Dispersive body waves: *J. Geophys. Res.*, **67**, 5279-5291.

Hu, C., Tu, N., and Lu, W., 2013, Seismic attenuation estimation using an improved frequency shift method: *IEEE Geosci. Remote Sens. Lett.*, **10**, 1026-1030.

Hu, W., Liu, J., Bear, L. and Marcinkovich, C., 2011, A robust and accurate seismic attenuation tomography algorithm, *81st Annual International Meeting, SEG, Expanded Abstracts*, 2727–2731.

Johnston, D. H., Toksoz, M. N., and Timur, A., 1979, Attenuation of seismic waves in dry and saturated rocks: II. Mechanisms: *Geophysics*, **44**, 691-711.

Kjartansson, E., 1979, Constant Q-wave propagation and attenuation: *J. Geophys. Res.*, **84**, 4137-4748.

Li, C., and Liu, X., 2015, A new method for interval Q-factor inversion from seismic reflection data: *Geophysics*, **80**, R361–R373.

Li, F., Zhou, H., Jiang, N., Bi, J. and Marfurt, K. J., 2015, Q estimation from reflection seismic data for hydrocarbon detection using a modified frequency shift method: *Journal of Geophysics and Engineering*, **12**, 577.

Li, F., Verma, S., Zhou, H., Zhao, T., and Marfurt, K. J., 2016a, Seismic attenuation attributes with applications on conventional and unconventional reservoirs: *Interpretation*, **4**, SB63-77.

Li, J., Wang, S., Yang, D., Dong, C., Tao, Y. and Zhou, Y., 2016b, An improved Q estimation approach: the weighted central frequency shift method: *Journal of Geophysics and Engineering,* **13**, 399-411.

Mittet, R., Sollie, R., and Hokstad, K., 1995, Prestack depth migration with compensation for absorption and dispersion: *Geophysics*, **60**, 1485–1494.

Picotti, S. and Carcione, J. M., 2006, Estimating seismic attenuation (Q) in the presence of random noise: *Journal of Seismic Exploration*, **15**, 165-181.

Quan, Y. and Harris, J. M., 1997, Seismic attenuation tomography using the frequency shift method: *Geophysics*, **62**, 895-905.

Raji, W. and Rietbrock, A., 2013, Attenuation (1/Q) estimation in reflection seismic records: *Journal of Geophysics and Engineering*, **10**, 045012.

Reine, C., Clark, R. A., and van der Baan, M., 2012, Robust prestack Q determination using surface seismic data: Part 1. Method and synthetic examples: *Geophysics*, **77**, R45–R56.

Tonn, R., 1991, The determination of the seismic quality factor Q from VSP data: A comparison of different computational methods: *Geophys. Prospect.*, **39**, 1-27.

Udias, A., 1999, *Principles of seismology*: Cambridge University Press.

Wang, S., and Chen, X, 2014, Absorption-compensation method by l1-norm regularization: Geophysics, **79**, no. 3, V107–V114.

Wang, S., Yang, D., Li, J. and Song, H., 2015, Q factor estimation based on the method of logarithmic spectral area difference: *Geophysics*, **80**, V157-V171S.

Wang, Y., 2002, A stable and efficient approach of inverse Q filtering: *Geophysics*, **67**, 657–663.

Wang, Y., 2006, Inverse Q-filter for seismic resolution enhancement: *Geophysics*, **71**, V51-V60.

Wang, Y., 2014, Stable Q analysis on vertical seismic profiling data: *Geophysics*, 79, D217–225.

Wang, Y., 2015, Frequencies of the Ricker wavelet: *Geophysics*, **80**, A31–A37.

Waters, K. H., 1978, *Reflection Seismology*: New York, Wiley.

Winkler, K. W., and Nur, A., 1982, Seismic attenuation: Effects of pore fluids and frictional sliding: *Geophysics*, **47**, 1–15.

Yan, H., and Liu, Y., 2009, Estimation of Q and inverse Q filtering for prestack reflected PP- and converted PS-waves: *Applied Geophysics*, **6**, 59-69.

Zhang, C., and Ulrych, T. J., 2002, Estimation of quality factors from CMP records: *Geophysics*, **67**, 1542–1547.

APPENDIX A

As an example, a Ricker wavelet is used to compare the amplitude spectrum and the power spectrum. We compute the amplitude spectrum and the power spectrum for a noise-free Ricker wavelet and noisy Ricker wavelet (Gaussian random noise is added to the noise-free Ricker wavelet, SNR = 15 dB) respectively. For convenience of comparison, the amplitude spectra and the power spectra are normalized, as displayed in Fig. A1. The solid lines show the amplitude spectrum and power spectrum for the noise-free Ricker wavelet, and the dotted lines for the noisy Ricker wavelet. We can observe that the amplitude spectra of noisy data deviates a lot from those of noise-free data at low and high frequencies. And there are large vibrations in the amplitude spectra of noisy data, particularly at high frequencies, which can greatly influence the Q estimation. By contrast, the power spectra of noisy data are relatively smooth and closer to the noise-free power spectra. This can demonstrate that power spectra is less sensitive to random noises than amplitude spectra.

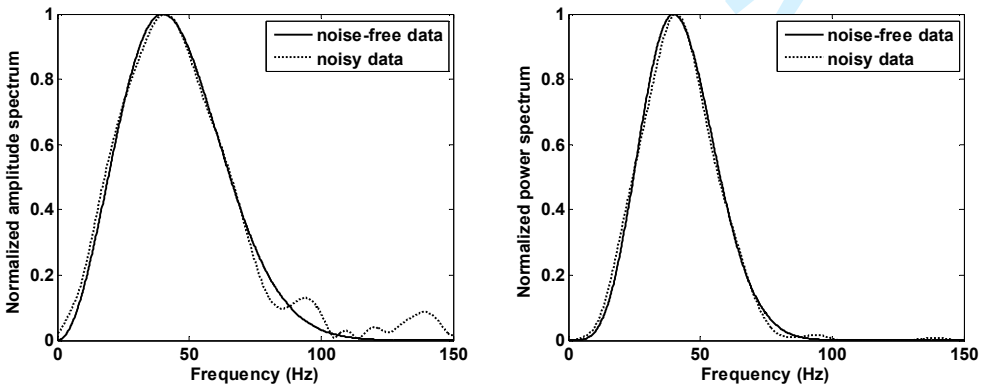

(a) (b)

Fig. A1. The amplitude spectra (a) and power spectra (b) of noise-free data and noisy data.

FIGURE CAPTIONS

Fig. 1: Synthetic data considering attenuation for different Q values when using Ricker wavelet (a), Gauss 1 wavelet (b) and Gauss 3 wavelet (c).

Fig. 2: Synthetic data considering attenuation for different travel time when using Ricker wavelet (a), Gauss 1 wavelet (b) and Gauss 3 wavelet (c).

Fig. 3: Noisy attenuation data when using Ricker wavelet (a), Gauss 1 wavelet (b) and Gauss 3 wavelet (c).

Fig. 4: Probability histograms of the estimated Q for Ricker wavelet when SNR is 20 dB (a, b) and 10 dB (c, d). 1000 independent realizations are performed. The actual Q is 100.

Fig. 5: Probability histograms of the estimated Q for Gauss 1 wavelet when SNR is 20 dB (a, b) and 10 dB (c, d). 1000 independent realizations are performed. The actual Q is 100.

Fig. 6: Probability histograms of the estimated Q for Gauss 3 wavelet when SNR is 20 dB (a, b) and 10 dB (c, d). 1000 independent realizations are performed. The actual Q is 100.

Fig. 7: Mean values (a) and standard deviations (b) of Q factors estimated by FWE and IFWE for different SNRs. 200 independent realizations are performed for each SNR. The true Q is 100.

Fig. 8: The relative errors of Q estimation using FWE and IFWE for synthetic data with SNR = 20 dB (b, c), 15 dB (d, e) and 10 dB (f, g) random noise for different bandwidth choices. The actual Q is 100. The noisy synthetic data is shown in (a).

Fig. 9: (a) A field VSP data set. (b) VSP down-going wavefields. (c) First arrivals of down-going wavefields. (d) First arrivals after inverse Q filtering. (e) Estimated Q for bandwidth 3-110 Hz. (f) Estimated Q for bandwidth 3-130 Hz. (g) Difference between (e) and (f). (h) Computed interval velocities from the first arrivals.

Fig. 10: (a) A field surface seismic section. (b) Compensated section after inverse filtering.

Fig. 11: (a) The 12th trace in the seismic section, which is subdivided into four parts: A, B, C and D for the purpose of Q estimation; (b) the time frequency spectra of this trace; (c) the estimated Q using the IFWE method.

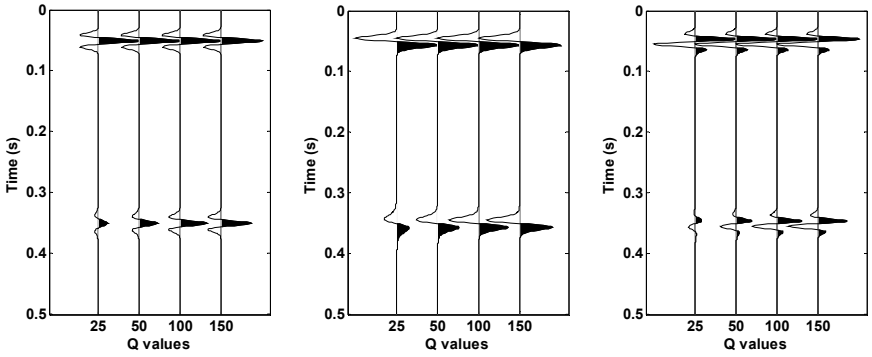

(a) (b) (c)

Fig. 1.

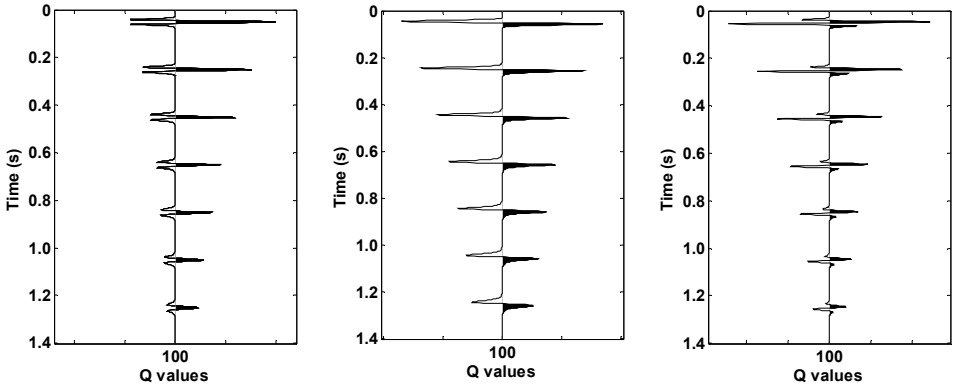

(a) (b) (c)

Fig. 2.

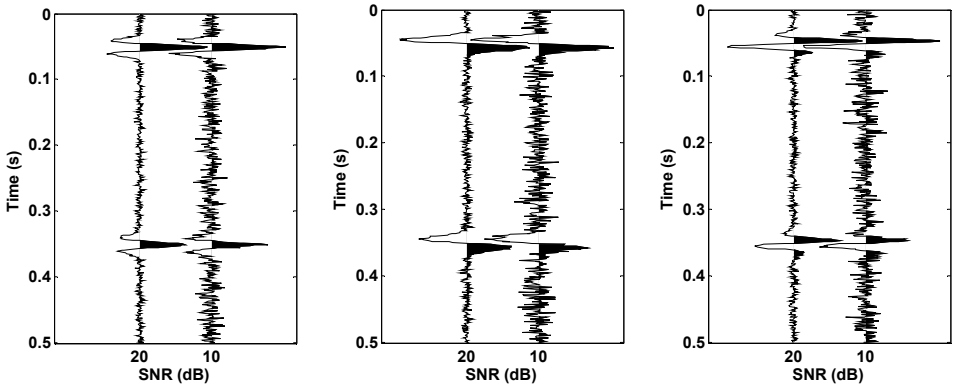

(a) (b) (c)

Fig. 3.

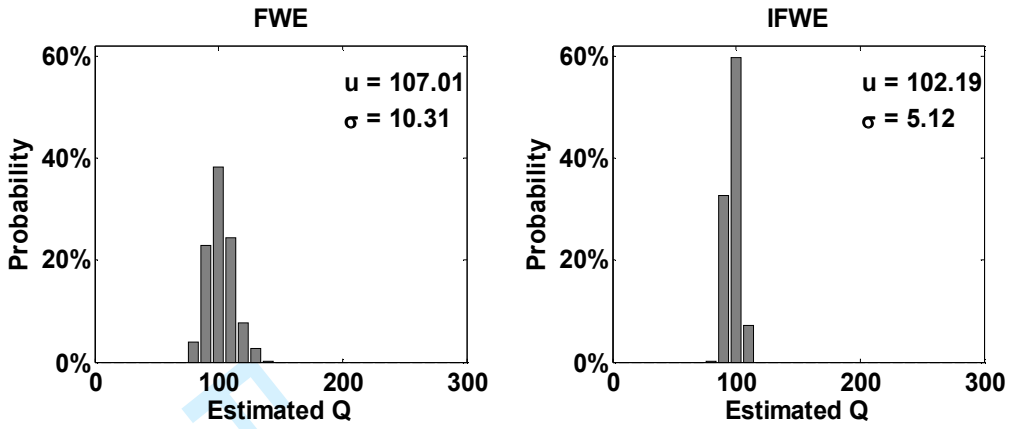

(a) (b)

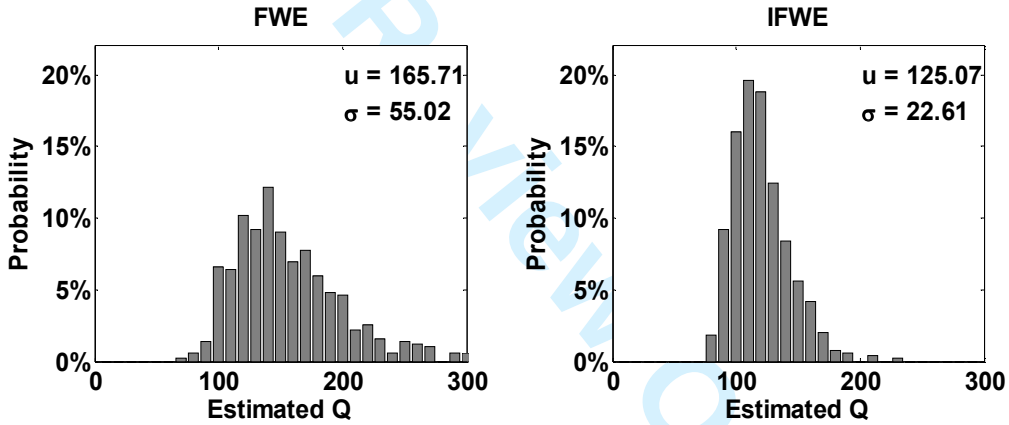

(c) (d)

Fig. 4.

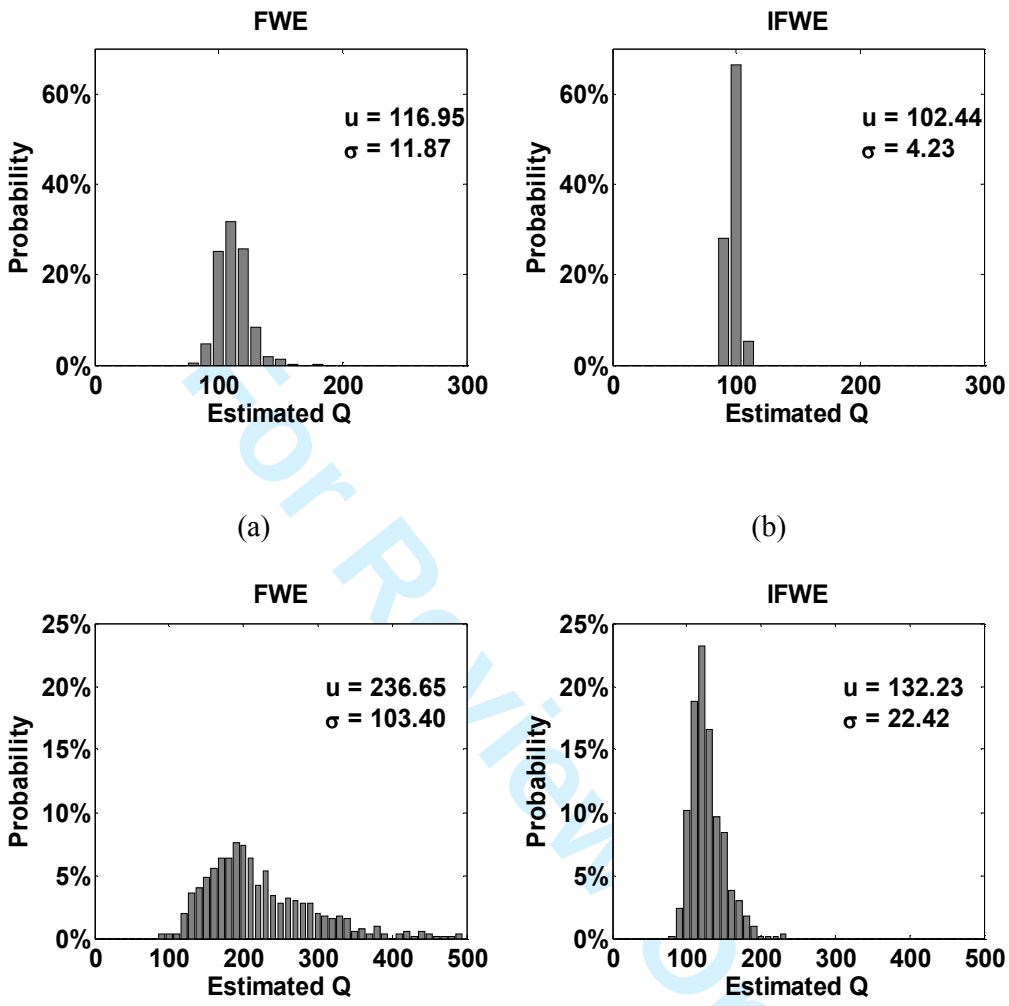

Fig. 5.

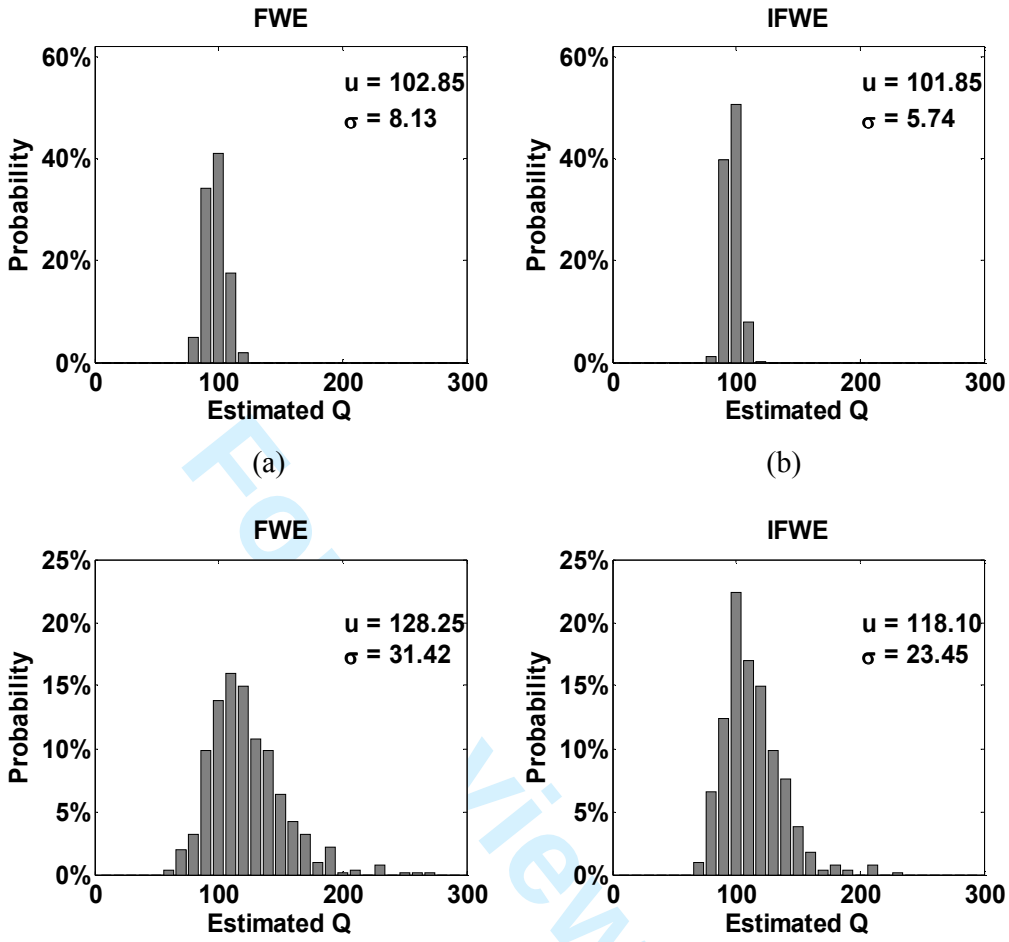

(a) (b)

(c) (d)

Fig. 6.

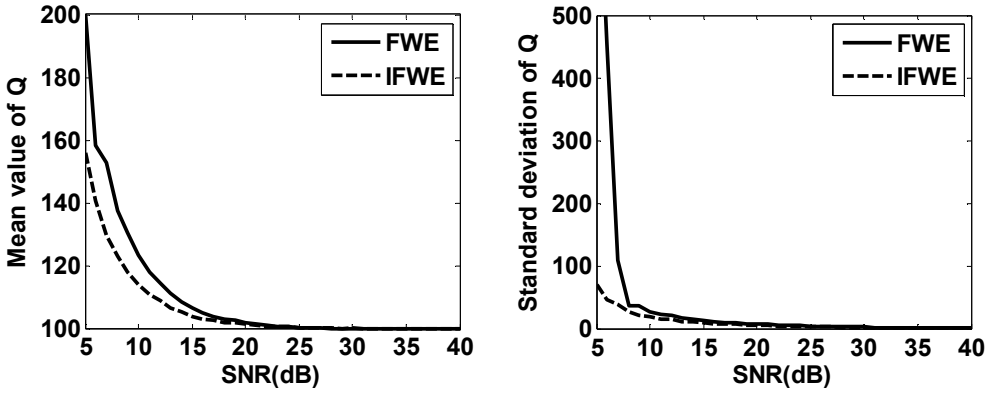

(a) (b)

Fig. 7.

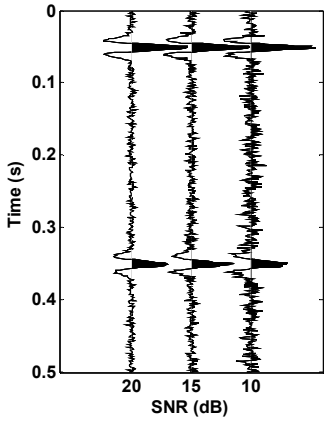

(a)

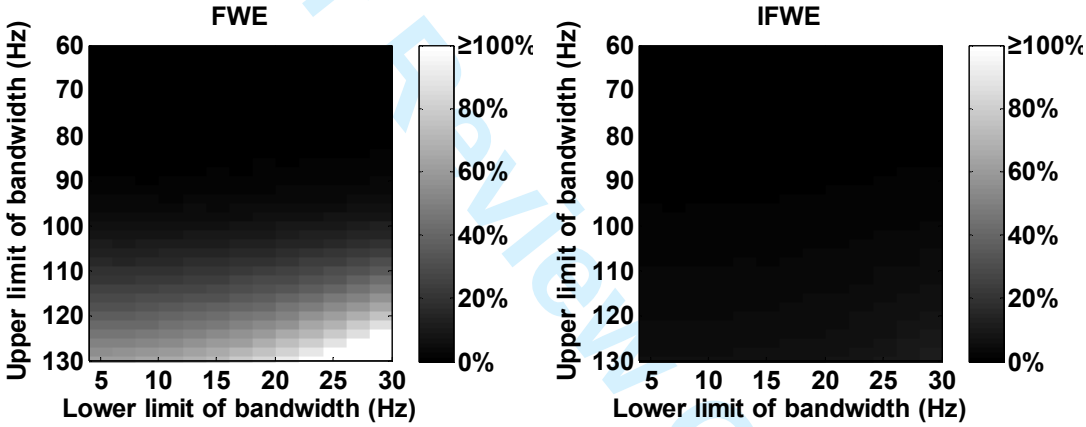

(b) (c)

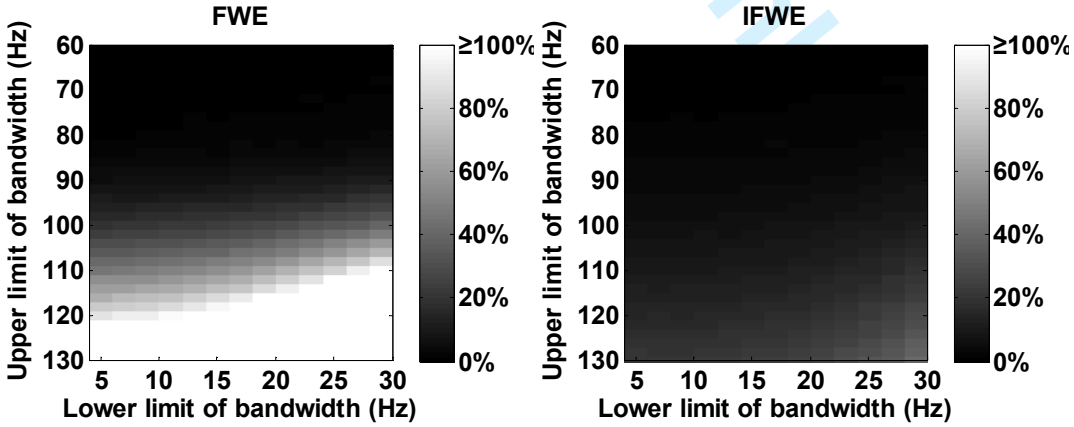

(d) (e)

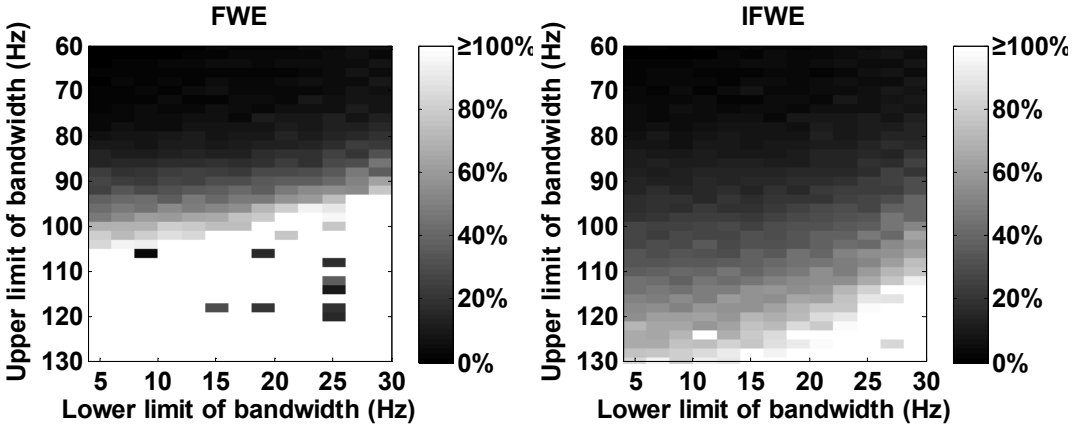

(f) (g)

Fig. 8.

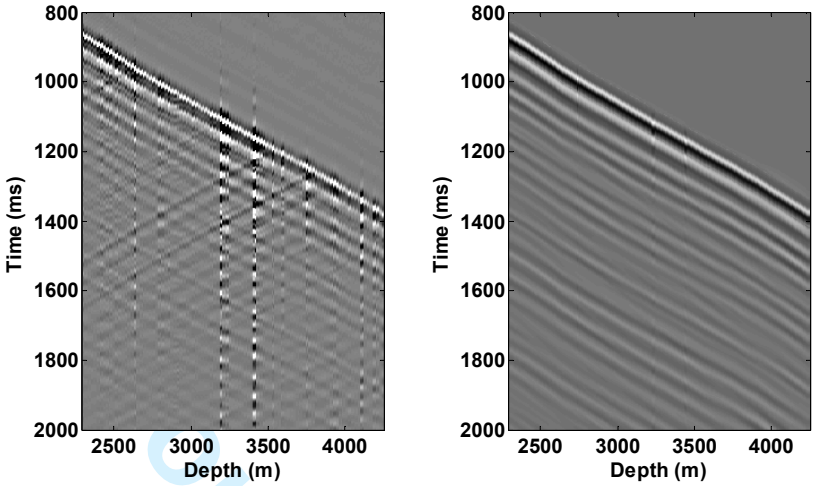

(a) (b)

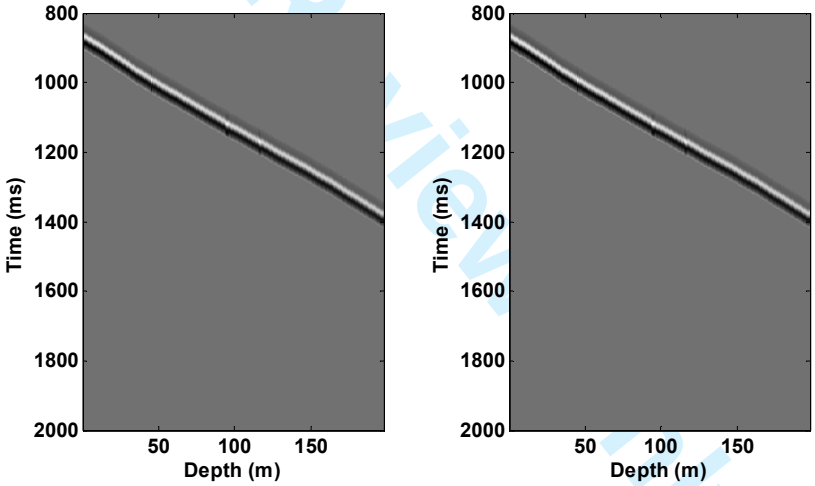

(c) (d)

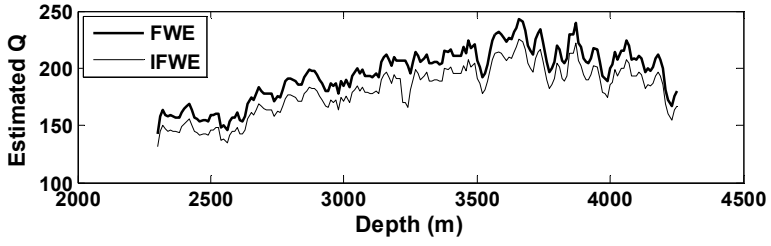

(e)

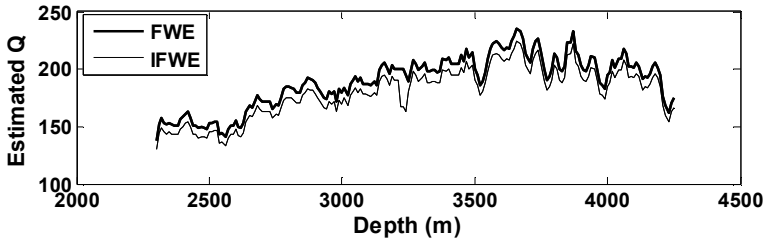

(f)

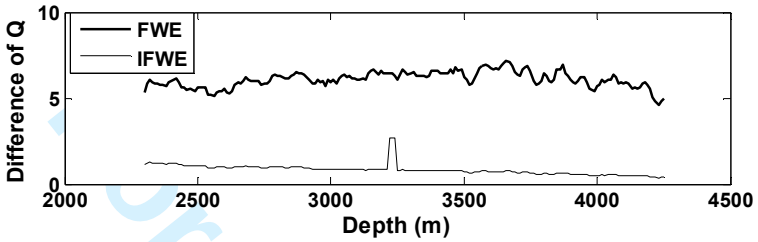

(g)

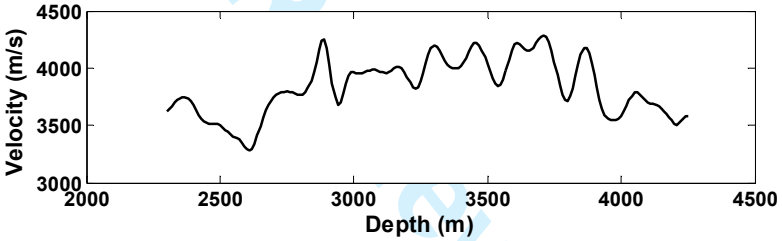

(h)

Fig. 9.

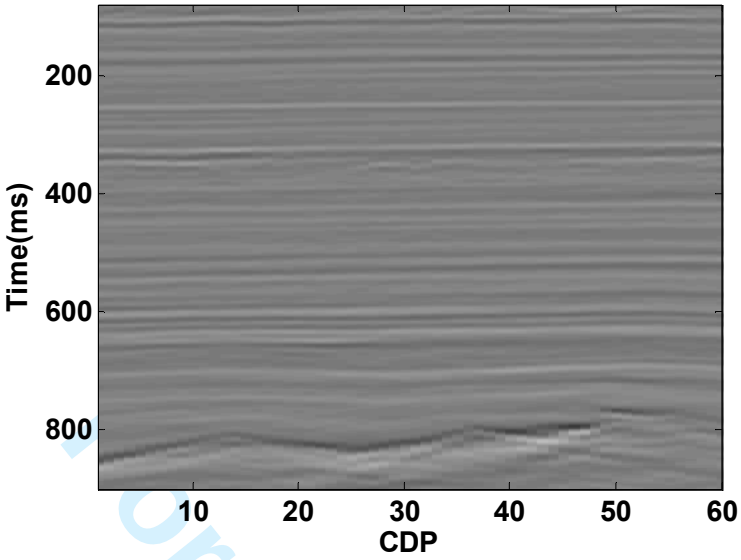
Time(ms)
200
400
600
800
10
20
30
40
50
60
CDP

(a)

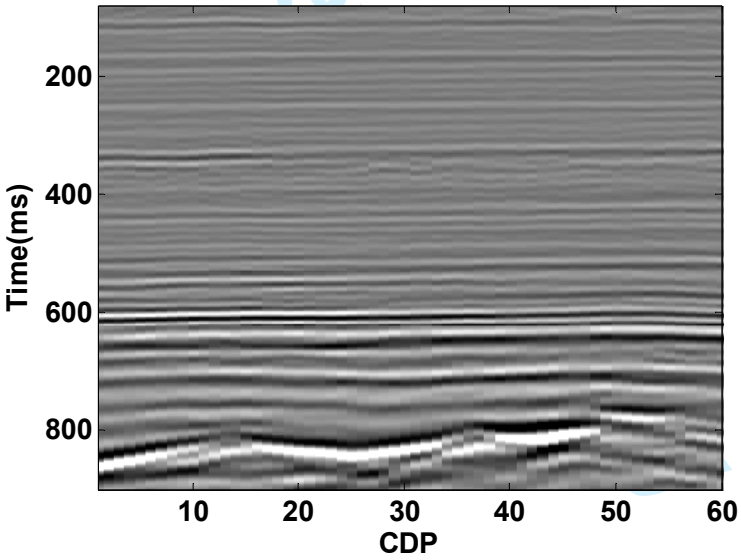
Time(ms)
200
400
600
800
10
20
30
40
50
60
CDP

(b)

Fig. 10.

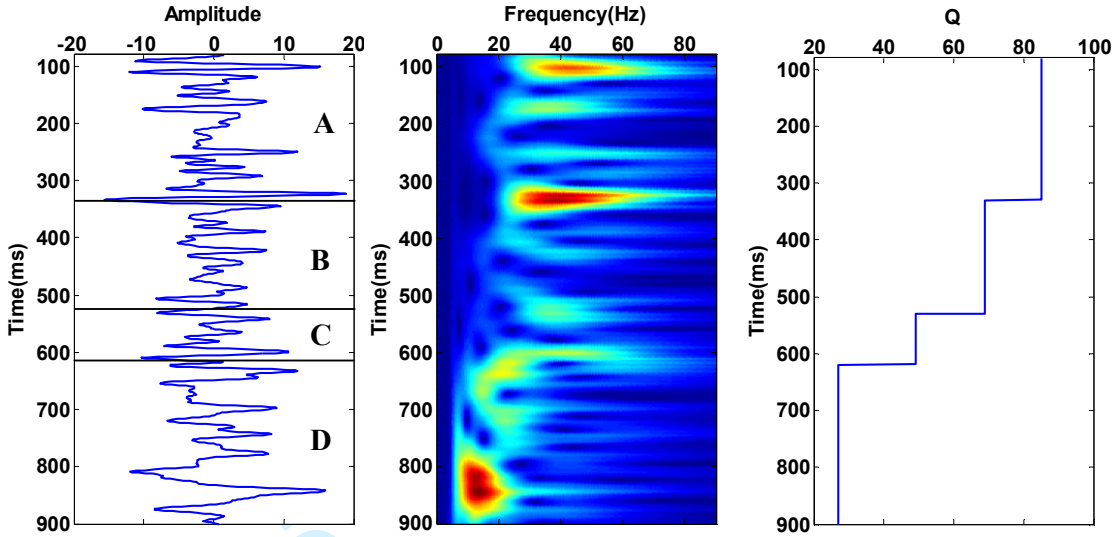

(a) (b) (c)

Fig. 11.

Table 1 Estimated Q for synthetic data using different wavelets. The travel time is 0.3 s.

	True Q	25	50	100	150
Ricker wavelet	CFS	28.93	53.54	103.32	153.24
	FWE	24.45	49.66	99.81	149.87
	IFWE	24.50	49.70	99.84	149.89
Gauss 1 wavelet	CFS	30.68	55.29	105.07	154.99
	FWE	24.45	49.66	99.81	149.87
	IFWE	24.34	49.60	99.78	149.85
Gauss 3 wavelet	CFS	27.57	52.16	101.93	151.85
	FWE	24.41	49.64	99.80	149.86
	IFWE	24.56	49.73	99.85	149.89

Table 2 Estimated Q according to original wavelet and attenuation wavelet at different travel time. The actual Q is 100.

	Time(s)	0.2	0.4	0.6	0.8	1.0	1.2
Ricker wavelet	CFS	102.16	104.53	107.08	109.80	112.69	115.71
	FWE	99.91	99.68	99.32	98.87	98.36	97.80
	IFWE	99.93	99.72	99.41	99.00	98.54	98.01
Gauss 1 wavelet	CFS	103.33	106.86	110.58	114.48	118.54	122.74
	FWE	99.91	99.68	99.32	98.88	98.36	97.80
	IFWE	99.90	99.62	99.20	98.67	98.05	97.38
Gauss 3 wavelet	CFS	101.23	102.68	104.32	106.14	108.14	110.28
	FWE	99.91	99.66	99.27	98.79	98.23	97.63
	IFWE	99.93	99.74	99.45	99.10	98.68	98.23